catalysts

MDPI

Article

Photocatalytic Properties and Chemical Durability of $CaO-B_2O_3-V_2O_5$ Borovanadate Glasses

Ayoub Kaaouass [1,*], Abdelkader Ben Ali [1], Hassan Ait Ahsaine [1,*], Ghizlaine Kaichouh [2], Abdelkader Zarrouk [2] and Mohamed Saadi [1]

[1] Laboratoire de Chimie Appliquée des Matériaux (LCAM), Faculty of Science, Mohammed V University in Rabat, Agdal-Rabat P.O. Box 1014, Morocco
[2] Laboratory of Materials, Nanotechnology and Environment, Faculty of Sciences, Mohammed V University in Rabat, Agdal-Rabat P.O. Box 1014, Morocco
* Correspondence: ayoubkaaouass@gmail.com or ayoub_kaaouass@um5.ac.ma (A.K.); h.aitahsaine@um5r.ac.ma (H.A.A.)

Abstract: The aim of this paper is to investigate the photocatalytic properties and chemical durability of the $CaO-B_2O_3-V_2O_5$ glasses system. The latter were synthesized by the melt-quenching technique. The amorphous nature of the prepared borovanadate glasses has been confirmed with X-ray diffraction. The chemical durability measured from their weights before and after immersion in deionized water and hydrochloric acid indicated that replacing V_2O_5 with B_2O_3 improved the chemical durability. The observed increases in chemical durability might be explained by the increase in the glass transition temperature, due to stronger bonding in the structural network. The photocatalytic performance was assessed by the degradation of methylene blue (MB) dye under irradiation, and the evolution of dye degradation was analyzed by UV-visible spectrometry. The vanadium content in the glass, the amount of catalyst, and the initial dye concentration showed a variable effect on the degradation of the MB dye. The photodegradation of methylene blue by the photocatalysts was found to follow pseudo-first-order rate kinetics. The photocatalytic activity for all the prepared photocatalysts showed a higher degradation performance, and the results indicated that 40 CaO-30 B_2O_3-30 V_2O_5 has the highest removal efficiency of about 99% in 180 min.

Keywords: borovanadate glasses; chemical durability; photocatalysis; transition metals; methylene blue dye

Citation: Kaaouass, A.; Ben Ali, A.; Ait Ahsaine, H.; Kaichouh, G.; Zarrouk, A.; Saadi, M. Photocatalytic Properties and Chemical Durability of $CaO-B_2O_3-V_2O_5$ Borovanadate Glasses. *Catalysts* **2023**, *13*, 512. https://doi.org/10.3390/catal13030512

Academic Editors: Bin Luo and Carolina Belver

Received: 14 November 2022
Revised: 23 February 2023
Accepted: 27 February 2023
Published: 2 March 2023

1. Introduction

Borate is one of the best materials for glass formation and the use of B_2O_3 as a network glass-forming oxide has many advantages: B_2O_3 forms two major structural units in borated glass networks, the triangle BO_3 and the tetrahedral BO_4 units, allowing the formation of anionic sites that accommodate various modified metal cations [1–4]. Additionally, vanadate (V_2O_5)-based glasses have attracted much interest in chemistry and materials science owing to their unique properties and applications in memory and switching devices [5,6]. Vanadate glasses are identified as n-type exceptional conductive properties due to the hopping between V^{4+} and V^{5+}.

The addition of transition metals (TMs) to borate glasses has attracted more attention because of their wide applications in industry, science, and medicine [3], as they exhibit good semiconducting properties [7]. Semiconductor glasses could be made from different transition metal oxides (e.g., V_2O_5, MoO_3, etc.) and the semiconducting properties of V_2O_5 glasses containing results from the hopping of 3 dL electrons between the V^{4+} and V^{5+} states [7–10]. For instance, borovanadate glasses have important properties, such as a low melting temperature, high chemical durability, and thermal resistivity, making them attractive materials for various applications [11].

Our previous investigation indicates that glasses of the CaO-B_2O_3-V_2O_5 system with compositions of 40 CaO-(60−x) B_2O_3-x V_2O_5 (x = 0–40 mol%) have a low melting temperature at 900–950 °C, and a low glass transition temperature (381–650 °C) that is dependent on the composition [12]. Suyeon Choi et al. [13] reported that when P_2O_5 is substituted with B_2O_3, the dissolution rates of the different glass systems decrease, with an increase in the B_2O_3 concentration. However, the addition of B_2O_3 has been reported to improve the chemical durability [13]. Recently, semiconductor materials have received much attention and are at the forefront of the environmental sector for their application in photocatalysis [14]. In recent decades, the development of photocatalysis technology has received increasing attention and is one of the most interesting topics for scientists who want to use it for the removal and degradation of organic pollutants [15–19].

So far, the presence of organic pollutants in water is one of the main problems confronting modern society, causing serious and irreparable damage to the natural world [20]. Even low concentrations of dyes in water cause a change in its color, and thus the penetration of light, which has several consequences [20,21]. Therefore, these dyes will need to be removed from the wastewater before discharge to natural waters. New materials with photocatalytic and removal properties are investigated for their efficient use [22,23]. In general, these materials are oxides based on metal cations with d0 or d10 configurations. These metals have also been reported to use visible light more efficiently than traditional photocatalysts such as TiO_2 [24–26]. Transition metal vanadium group-5, block-d, is one of these metallates. V_2O_5 has a bandgap energy of 2.3 eV in the visible region, which shows high reactivity for the photocatalytic reaction [14,27]. Recent studies on bismuth vanadate ($BiVO_4$) [24,28], vanadium pentoxide (V_2O_5) [14], and zinc vanadate nanoparticles [29] revealed that these phases are semiconducting photocatalysts which exhibit good degradation efficiency. Studies using glasses and glass-ceramics as photocatalysts for wastewater treatment have been widely reported recently [30–36]. Herein, we have used the prepared materials as photocatalysts for the removal of methylene blue (MB) as a model pollutant in aqueous medium. MB is a thiazine dye that can cause eutrophication of surface waters [37], and it is characterized with a deep blue color and widely used in industry. This dye can have harmful effects on human health and our ecosystem. It can cause methemoglobinemia, vomiting, nausea, and tissue necrosis [37,38].

In this work, glass materials with different compositions of CaO-B_2O_3-V_2O_5 were successfully prepared. The chemical resistance of these glasses was examined in two solutions with different initial pH values, and the obtained results show how B_2O_3 influences the chemical durability in the glass system. Thus, the photocatalytic efficiency of the synthesized glasses was investigated by monitoring the degradation of methylene blue with various concentrations in an aqueous medium under illumination.

2. Experimental Procedures

2.1. Sample Preparation

Calcium borovanadate glasses with compositions of 40 CaO-(60−x) B_2O_3-x V_2O_5 (with x = 0, 10, 20, 30 mol%) were synthesized by a conventional melt-quenching method from stoichiometric mixtures of vanadium oxide (V_2O_5), boric acid (H_3BO_3), and calcium carbonate ($CaCO_3$). These starting products were precisely weighed and thoroughly ground in the agate mortar to homogenize the batch before being heated at 400 °C to remove volatile organic species. Then, the mixtures were gradually heat-treated at 900–950 °C for about 60 min. The melted liquid obtained was quenched in a steel mold preheated to around 200 °C.

Different methods were used to characterize the obtained glasses, namely density measurement and thermal analysis by differential scanning calorimetry (DSC), as reported in the previous work [12]. The compositions of the prepared glasses are provided in Table 1 with the values of density and glass transition temperature. For confirmation of the vitreous nature of each glass sample, X-ray diffraction diagrams were recorded and reported in our earlier paper [12].

Table 1. Composition (mol %), density ρ (g·cm^{-3}), glass transition temperature Tg (°C), and dissolution rate (DR) (g/cm^2/min) of the studied glasses.

Glass No.	CaO	B_2O_3	V_2O_5	ρ [12]	Tg ± 6° [12]	DR (pH = 7)	DR (pH = 4)
A1	40	60	0	2.603	650	$(3.76 \pm 0.20) \times 10^{-7}$	$(4.74 \pm 0.20) \times 10^{-7}$
A2	40	50	10	2.669	570	$(1.58 \pm 0.20) \times 10^{-6}$	$(4.18 \pm 0.20) \times 10^{-6}$
A3	40	40	20	2.749	480	$(2.05 \pm 0.20) \times 10^{-6}$	$(6.74 \pm 0.20) \times 10^{-6}$
A4	40	30	30	2.853	430	$(5.48 \pm 0.20) \times 10^{-6}$	$(8.95 \pm 0.20) \times 10^{-6}$

2.2. Durability Testing

To assess the chemical durability, the prepared samples were polished, cleaned, and weighed with an analytical digital balance. Then, the glass samples were attacked and completely immersed at room temperature for 28 days in deionized water (pH = 7) and for 5 days in an acidic HCl solution (pH = 4). The weight of each glass sample was measured after its immersion at regular intervals (144 h, 288 h, 432 h, 576 h, 672 h) in deionized water and (24 h, 48 h, 72 h, 96 h, 120 h) in an acidic HCl solution. The percentage of weight loss (WL) was determined from the following formula [39,40]:

$$WL = \frac{WB - WA}{WA} \times 100 \quad (1)$$

where WA and WB are the weights of the glass after and before immersion in the solution.

Therefore, the dissolution rate was found from the weight loss with the expression [41,42]:

$$DR = \frac{\Delta W}{A.t} \quad (2)$$

where ΔW is the weight loss (g), A is the area (cm^2) before dissolution, and t is the immersion time (min).

To see the effect of vanadium on the vibrational properties and according to our previous work [12], in infrared spectroscopy, there is a small band situated in the 1200–1600 region, and the maximum at 1230 cm^{-1} starts to appear when the molar content of V_2O_5 exceeds 10%, which is explained by the presence of diborovanadate $[B_2V_2O_9]^{2-}$ groups [43,44]. Furthermore, from the Raman spectra [12], the absence of a peak in the range 930–947 cm^{-1} for the sample that is not containing V_2O_5 is normal as there is no V = O bond, while when V_2O_5 was added, this peak began to appear, which is attributed to the V = O vibrations of the tetrahedral units VO_4 or VO_5 [12,45].

The formation of diborovanadate groups is clarified by assuming that in glasses containing more than 10 mol% V_2O_5, a continuous random lattice is formed of either two BO_4 units and two VO_4 units or two BO_3 units and two VO_5 units, and the construction was proposed by Reddy and co-workers for the diborovanadate $[B_2V_2O_9]^{2-}$ [43,44]. From the IR, Raman results, and the proposed structure construction, we infer that the V^{5+} content of the total vanadium in the structure has the highest proportion (see Supplementary Information).

2.3. Photocatalyic Activity

The photocatalytic degradation was performed in a circular quartz vessel under continuous UV exposure. The glass samples were irradiated with a 125 W Philips mercury vapor lamp (λ = 254 nm). Methylene blue (MB) was chosen as an organic pollutant for the photocatalytic degradation experiments. It is a representative strong cationic dye that has been extensively used as an organic model to examine the photocatalytic performance of photocatalysts [46–48]. For this, 150 mL of aqueous solution containing different concentrations of MB was suspended with each powder of the glass samples as photocatalysts. The distance between the lamp and the beaker is 10 cm. Before illumination, the solution was kept in the dark and under stirring for 45 min to establish adsorption/desorption,

reaching the equilibrium. Afterward, the solution was irradiated to start the photocatalysis reaction. At the designated times, samples of the solution were taken and their UV-visible absorption spectra were measured to evaluate the photocatalytic degradation using a Jasco V-730 (Japan) UV-visible spectrophotometer (UV-2300). The 664 nm absorption band (Figure 1) represents the maximum absorbance of the methylene blue, and the change in MB concentration will be monitored at λ = 664 nm. The percent of MB dye degradation was obtained from the concentration difference, as shown in Equation (3) [49]:

$$\text{Photocatalytic efficiency} = \left(1 - \frac{C}{C_0}\right) \times 100 \quad (3)$$

C_0: the initial concentration of MB dye,
C: the concentrations of the solutions after irradiation.

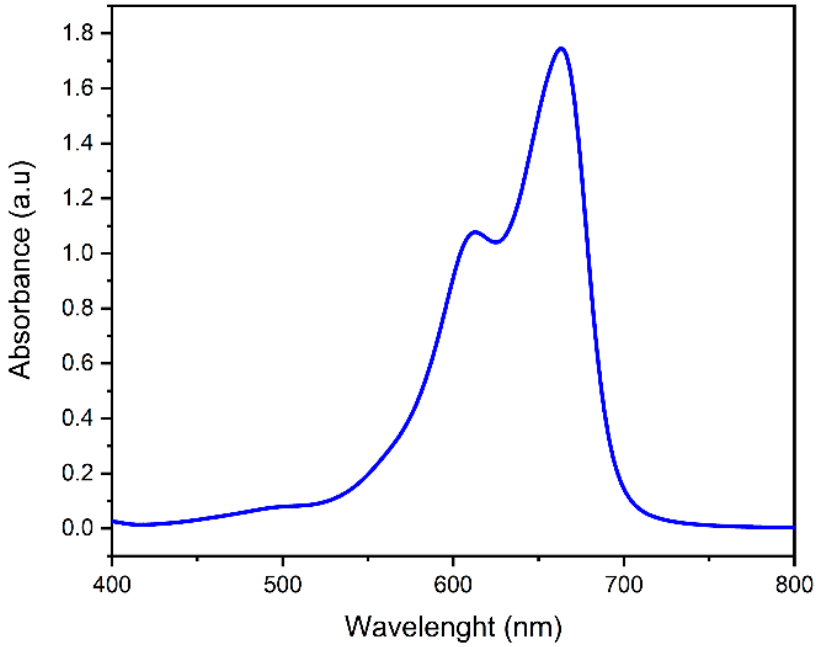

Figure 1. Absorbance spectrum of MB.

3. Results and Discussion

3.1. Chemical Durability

3.1.1. Variation in Weight Loss and Dissolution Rate (DR)

Figure 2a,b illustrate the weight loss percent versus the leaching time in deionized water and in HCL solutions, respectively. As one can see, the mass loss increases proportionally with the immersion time. In deionized water (Figure 2a), the mass loss is dependent on the prepared sample, and different trends were recorded. Sample A4 containing less boron and more vanadium rapidly increased, reaching 43% in 720 h. On the other hand, sample A1, which has the highest percentage of boron, showed an increase in percentage weight loss of only 2% during the immersion time. However, for A2 and A3 samples, a similar weight loss behavior was observed, recording around 10% and 14% at 720 h, respectively.

In HCl solution, we observed a similar tendency: During 24 h, all samples showed a low weight loss which did not exceed 2%. After a long immersion time of more than 50 h, we noticed that:

1. The weight loss of sample A4 rapidly increased to reach 11% in 120 h.
2. The sample A1 showed a very low weight loss of nearly 1% in 120 h.
3. A similar weight loss of 5% was recorded for A2 and A3 samples.

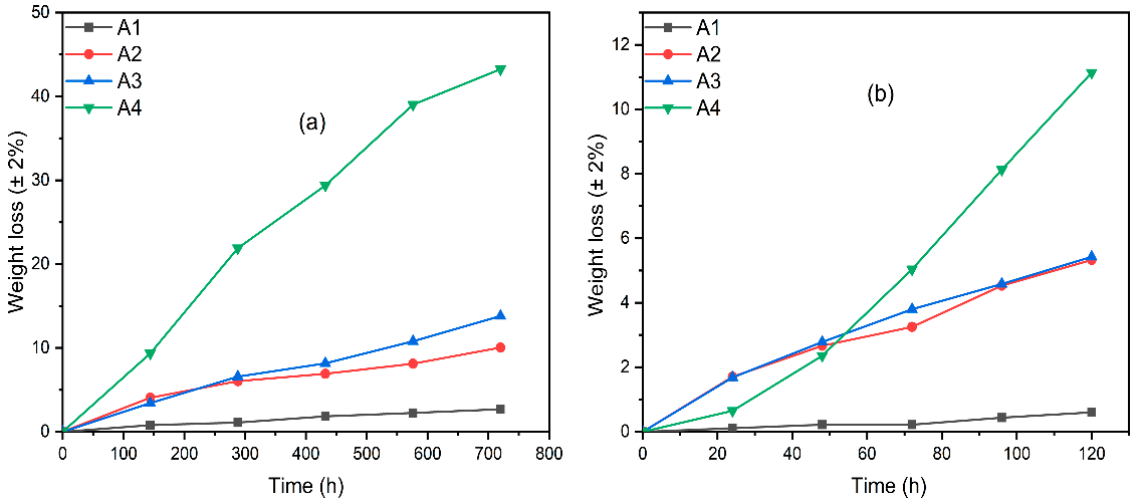

Figure 2. Changes in weight loss of different glass samples in deionized water (**a**) and in HCl solution (**b**).

The increase in weight loss with the increasing immersion time is assigned to the fact that the glass components had adequate time to be liberated into the solution [40]. The increase of the weight loss of the sample A4 might be due to different reasons. For instance, the high content of B_2O_3 and/or V_2O_5 as well as the value of the glass transition temperature are the main factors that influence the weight loss. Below, we have found the dissolution rates of the four samples.

Figure 3a,b show the dissolution rate (DR) of glasses as a function of B_2O_3 content, after 720 h and 144 h of the leaching test in different solutions: deionized water (pH = 7) and HCl (pH = 4), respectively.

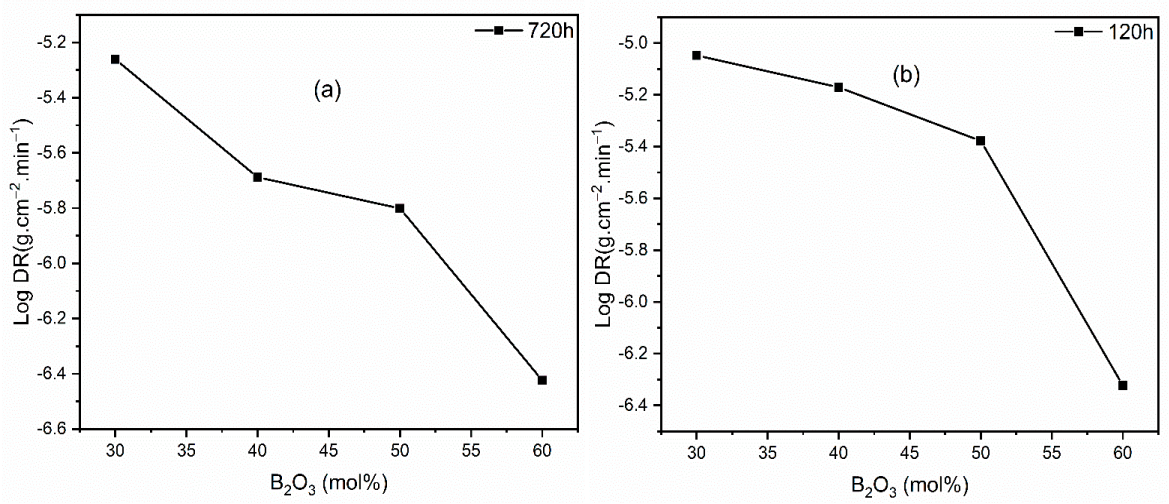

Figure 3. Changes in the dissolution rate (DR) versus the composition of 40 CaO-(60−x) B_2O_3-x V_2O_5 glasses (x = 0, 10, 20, and 30 mol%) after immersion in deionized water (**a**) and in HCl solution (**b**).

In an acidic medium (Figure 3b), the dissolution rate slightly decreased between 30 and 50 molar% of B_2O_3. When more than 50% B_2O_3 was added, the dissolution rate rapidly decreased. In our case, we supposed that the lower DR for more than 50% B_2O_3 corresponds to the absence of diborovanadate groups in the solution [12]. According to our previous work [12], diborovanadate groups are present in glasses containing more than 10% V_2O_5 and less than 50% B_2O_3. Thus, the addition of less than 50 mol% B_2O_3 indicates that B_2O_3 has a lesser effect on the glass structure. A similar effect was found for minor additions of MnO in (50−x) K_2O-x MnO-50 P_2O_5 glasses [50]. Furthermore, when the samples were immersed in deionized water (Figure 3a), the DR was also reduced at

the immersion time of 720 h. In general, the dissolution rate depends on the chemical compositions, bond forces, bond lengths, and the number of the coordination of atoms in the glass matrix [39,40]. The increase in the glass transition temperature with increasing B_2O_3 content (Table 1) led to a higher chemical durability due to increased cross-linking between the borate chains, and therefore a stronger bond in the structural network [51–53]. The results of the DR show that the increase in B_2O_3 content of borovanadate glasses led to a more effective chemical durability improvement. Addition of B_2O_3 has been reported to improve the chemical durability in several works [13,53,54]. As can be seen from Table 1, A1 glass has the lowest DR value (3.76×10^{-7} and 4.74×10^{-7} g/cm^2/min in deionized water and HCL, respectively), which is quite close to that of window glasses ($10^{-7.2}$–$10^{-8.4}$ g/cm^2/min) [41,55,56], and to those (1.1×10^{-7}–6.6×10^{-9} g/cm^2/min) of iron phosphate waste-forms [41,55].

According to Suyeon Choi et al. [13], the greater DR of glass systems containing high concentrations of V_2O_5 (70 V_2O_5-x B_2O_3-(70−x) P_2O_5) confirms that V_2O_5 does not enhance the chemical durability, which is in good agreement with our results.

3.1.2. Variation of the pH

Figure 4a,b show the evolution of the pH value as a function of immersion time in water and HCl, respectively, for all prepared glasses. In acidic solution (Figure 4b), we found that the pH curves consist of two regions: The first region occurs before 24 h, with a fast increase in the pH of the solution resulting from the sudden ion exchange between the glass and the solution [50,52]. The second region is between 24 h and 120 h, exhibiting a plateau that can be assigned to the saturation of the surrounding solution [57]. An identical pH behavior was observed in water (Figure 4a). However, small pH fluctuations around 8–9 were noted in the studied timespan.

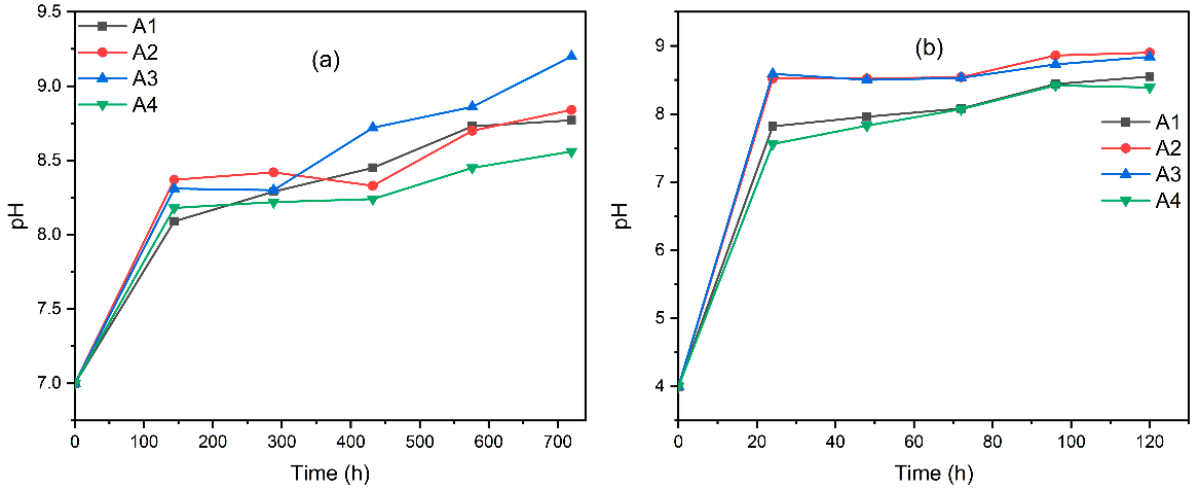

Figure 4. pH variation versus immersion time of the prepared glasses in deionized water (**a**) and in HCl solution (**b**).

The pH increases of the leaching solutions (HCl pH = 4 and deionized water pH = 7) could be ascribed to the extraction via ion exchange processes between the solution's proton and the lattice-modifying elements. This exchange process is behind the obtained pH values because of the increase of OH^- ions remaining in the solution [50,52].

3.2. Photocatalytic Activity

3.2.1. Effect of V_2O_5 and Modeling of Photodegradation Kinetics

The photocatalytic reaction was performed by choosing methylene blue as the model organic pollutant. The prepared materials of CaO-B_2O_3-V_2O_5 glasses with different percentages of vanadium have been used as photocatalysts under UV light conditions. Generally, under illumination, the catalyst leads to the creation of a hole (h^+) in the valence band and

an electron (e^-) in the conduction band (CB). The electron (e^-), before being recombined with the hole, reacts with the water molecule on the surface to create OH^- radicals. These radicals lead to the degradation of organic molecules [30,58,59].

Figure 5a illustrates the photocatalytic tests for MB (10 mg/L) degradation in the presence of the three borovanadate glass catalysts. As the figure shows, the concentration of MB is reduced with the irradiation time in the presence of different catalysts. This decrease is dependent on the vanadium percentage. Photocatalytic performance was enhanced as the nominal vanadium oxide content increased, reaching the highest MB decolorization for the 40Ca0-30B_2O_3-30V_2O_5 photocatalyst. The decrease in MB concentration in the dark was a result of adsorption, whereas that under illumination occurred as a result of both adsorption and decomposition of MB [60]. After the reaction time, there was almost complete removal of the MB molecule. Over 99% of MB was photo-decomposed, confirming the excellent photocatalytic performance of the 40Ca0-30B_2O_3-30V_2O_5 catalyst. Furthermore, the percentages of degradation for the other catalysts, 40 CaO-(60−x) B_2O_3-xV_2O_5 with x = 20 and x = 10, were 96% and 84%, respectively (Figure 5b). It can be observed from previous studies [61–63] that the addition of vanadium with an optimal amount improves the photocatalytic activity.

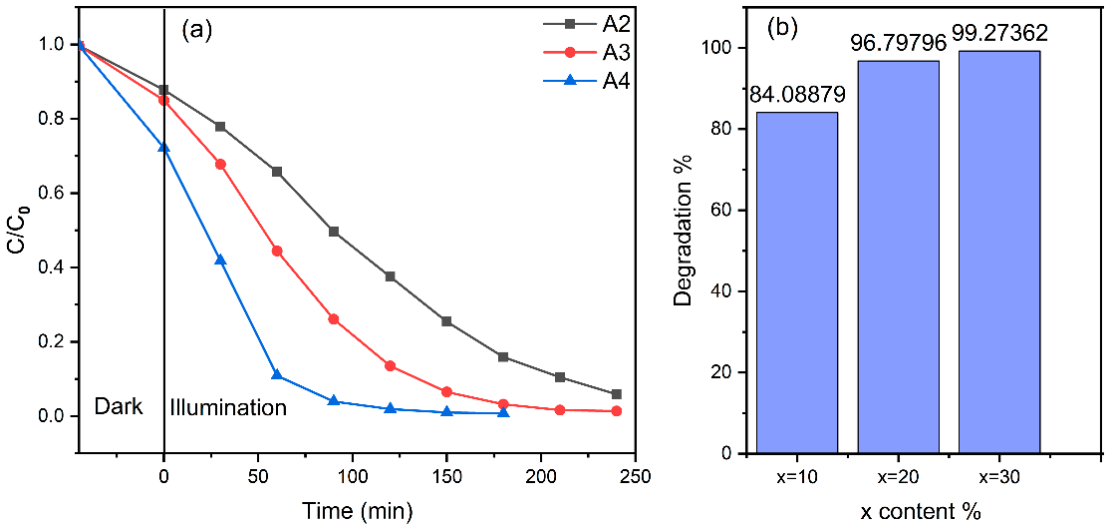

Figure 5. Degradation efficiencies of prepared glasses: (**a**) plot of C/C_0 versus time t and (**b**) percentage of MB degraded after 180 min.

The kinetic rate is an importance parameter for degradation studies as it could predict the rate at which a pollutant is eliminated from the water solution. For this purpose, the kinetic characteristics of the different glasses used as photocatalysts for the photodegradation of methylene blue were carried out. Figure 6a shows the kinetic fitting curves of ln (C_0/C) versus irradiation time, t, for the different photocatalysts, which indicate that the degradation follows a pseudo-first-order kinetics obtained from the Langmuir–Hinshelwood equation [64–66]:

$$\mathrm{Ln}\left(\frac{C_0}{C}\right) = k.t \quad (4)$$

where C_0 is the initial MB concentration, C is a concentration of MB at any time, t, k is the rate constant for the first order, and t is time.

The rate constants are presented in Figure 6b, allowing a quantitative comparison to represent the photocatalytic activity. According to the figure, it can be clearly observed that the constant rate was significantly enhanced from 0.0113 min^{-1} to 0.0274 min^{-1} by raising the V_2O_5 content from 10% to 30%, which accounts for an almost 2.5-fold increase in the catalytic efficiency. In addition, it can also be noticed that the 40 CaO-30 B_2O_3-30 V_2O_5 photocatalyst presented the greatest constant k value. From the kinetic data, it was concluded

that as the content of vanadate increased, the constant rate was improved, indicating that vanadium is a key parameter to enhance the photodegradation process.

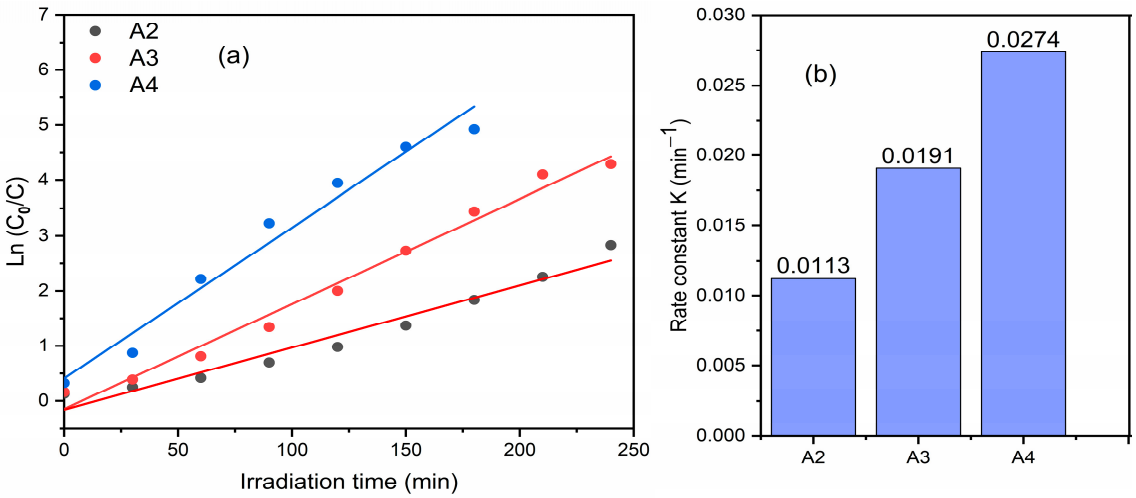

Figure 6. (**a**) Pseudo-first-order kinetics and (**b**) the rate constant k of the photocatalysts.

The high rate constant observed for the A4 sample can be principally due to the change in morphologies, and voids in the glass matrix. This enhanced the MB adsorption and yielded more active sites for the photocatalytic degradation of MB molecules [67]. The existence of vanadium oxide promoted the migration of photogenerated electrons to vanadium, thereby enhancing the electron–hole separation [62].

3.2.2. Effect of Catalyst Loading and of Initial MB Concentration

The effect of catalyst mass on the MB photodegradation was examined. In this regard, we have selected the best-performing photocatalyst (40 CaO-30 B_2O_3-30 V_2O_5) at different loadings ranging from 0.5 to 3 g/L. Figure 7 displays the obtained results. In the dark, the highest adsorption amount was around 44%, recorded by a catalyst amount of 3 g/L. Other loadings have recorded around 30% of MB adsorption. Once the irradiation was turned on, the 3 g/L catalyst loading showed the fastest degradation rate, explained by its higher MB uptake in the dark through the adsorption process. After 90 min of irradiation, a 1 g/L loading recorded the lower degradation efficiency compared to 0.5, 2, and 3 g/L. Interestingly, the 1 g/L loading has also showed the lowest adsorption uptake in the dark, and this explains its low active sites availability and hence low photocatalytic activity compared to the other loadings. The small decrease of the photocatalytic efficiency of the 1g/L loading compared to the 0.5 g/L loading can be explained by the fact that the light transmission field decreased as the opacity of the solution increased [15,33].

Keeping the catalyst loading of 40 CaO-30 B_2O_3-30 V_2O_5 constant at 0.5 g/L, the effect of various initial MB concentrations on the photocatalytic activity is presented in Figure 8. The initial dye concentration was varied in the range of 5 to 15 mg L^{-1}. During the adsorption process, when the MB concentration increased, the removal efficiency of MB decreased. After illumination, we observed that MB degradation with the 15 mg/L concentration was the slowest. This was expected due to the higher amount of the dye and the low-light transmission field. This can also be explained by the large quantity of simulated illumination absorbed by MB molecules, more than by the catalyst at high MB concentrations [15,68]. The catalyst with different concentrations of MB (5, 10, and 15 mg/L) reached almost the same degradation value around 99% during 180 min of irradiation.

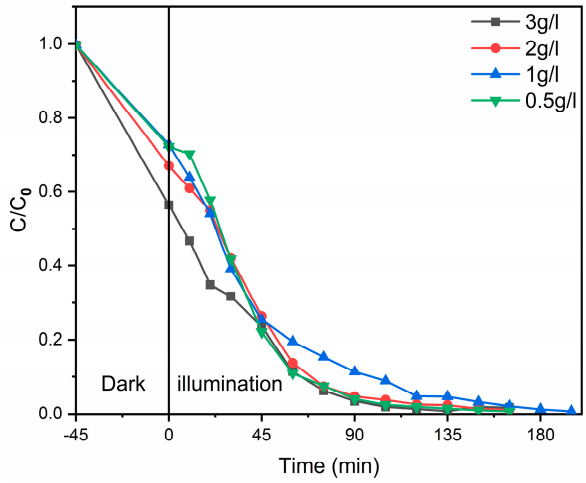

Figure 7. Photocatalytic degradation of MB (10 mg/L) at various catalyst loadings of 40CaO-30B_2O_3-30 V_2O_5 glass.

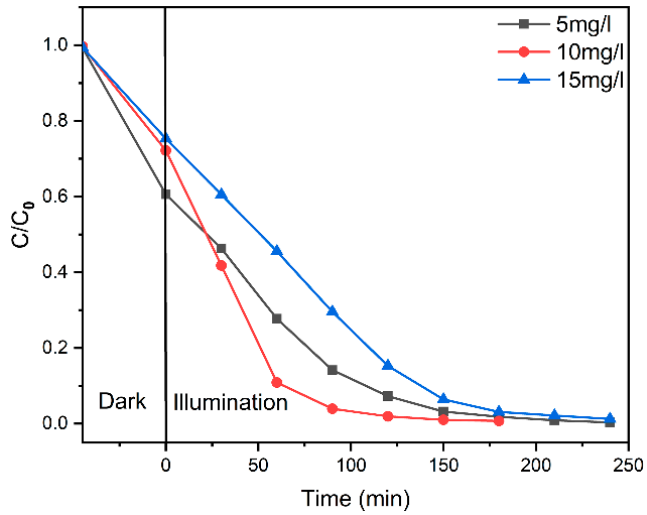

Figure 8. Photocatalytic degradation of methylene blue at different initial MB concentrations with 40 CaO-30 B_2O_3-30 V_2O_5 catalyst.

Figure 9 shows the evolution of the UV-vis absorption spectrum as a function of the photodegradation time of the MB dye for the best-performing catalyst, 40 CaO-30 B_2O_3-30 V_2O_5 glass (0.5 g/L), at the optimal conditions of catalyst amount and dye concentration. As can be seen from Figure 9, the color of the 10 ppm MB solution completely disappeared after 180 min of illumination.

In order to further investigate the photocatalytic mechanism, the main active species generated during the process of MB degradation were inspected by the scavenging experiments.

The scavenging tests for hydroxyl radicals, superoxide ions, and holes were performed using isopropanol, ascorbic acid, and EDTA, respectively [69–72]. Figure 10 shows the effect of these scavengers on the degradation of MB. We found that in the presence of EDTA and ascorbic acid, the degradation efficiency was reduced to 43% and 39%, respectively. However, a low inhibition was observed for MB degradation with the addition of isopropanol (70%). Thus, it could be inferred that h^+ holes and $O_2\bullet^-$ ions should be the dominant active species in the photocatalysis of MB, while hydroxyl radicals play a minor role in the photocatalytic reaction. Since the reduction potential of photogenerated electrons from the photocatalyst was higher than that of $O_2\bullet^-/O_2$ (0.28 eV), the released electrons can be easily transferred to oxygen (O_2) molecules adsorbed on the surface of the borovanadate photocatalyst, producing the superoxide $O_2\bullet^-$, which is a strong oxidizing species to degrade organic molecules.

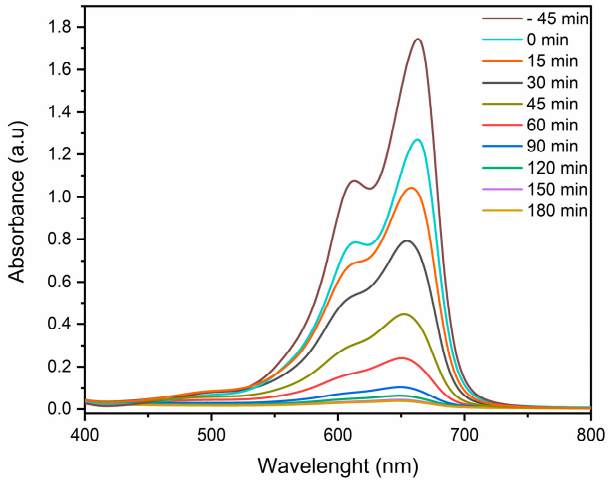

Figure 9. UV-vis absorption spectra changes of MB (10 mg/L) solution at various times by 40CaO-30 B_2O_3-30 V_2O_5 (0.5 g/L).

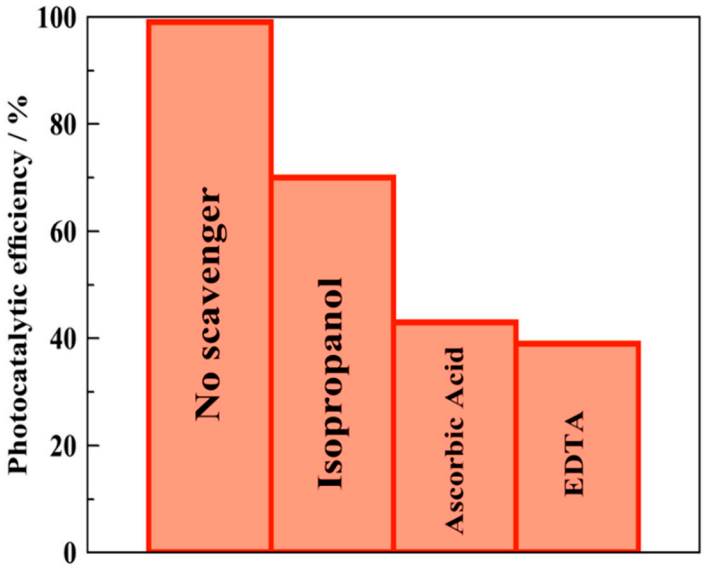

Figure 10. The effect of the scavengers on MB degradation.

Table 2 reports the comparison with state-of-the-art photocatalysts for MB photocatalytic degradation. As one can see, the efficiency presented in this paper is one of the most promising catalysts for MB removal.

Table 2. Comparison with the state-of-the-art photocatalysts for MB degradation.

Catalyst	Concentration of Catalyst	Concentration of Dye	Light Source	Photocatalytique Degradation	Ref
$Zn_3(VO_4)_2/BiVO_4$	0.7 g/L	-	Visible light	98% at 90 min	[73]
CuO-$BiVO_4$	0.6 g/L	10 mg/L	Visible light	92% at 240 min	[74]
$SrBi_3VO_8$	0.17 g/L	10 mg/L	Visible light	80% at 180 min	[75]
$2Bi_2O_3$–B_2O_3 (BBO) glass		50 mg/L	UV light	25% at 180 min	[36]
Fe doped TiO_2	1 g/L	10 mg/L	UV light	38% at 120min	[64]
CdS-Borosilicate glass (SiO_2-B_2O_3-Na_2O-ZnO)	1 g/L	10 mg/L	sunlight	68% at 270 min	[34]

Table 2. *Cont.*

Catalyst	Concentration of Catalyst	Concentration of Dye	Light Source	Photocatalytique Degradation	Ref
titanium-doped hydroxyapatite	0.5 g/L	10 mg/L	UV light	99% at 240 min	[76]
SnO_2/CdSe/Bi_2S_3 composite	0.5 g/L	30 mg/L	Visible light	99% at 60 min	[77]
Tin Oxide (SnO_2)	0.5 g/L	30 mg/L	Visible light	53% at 60 min	[77]
CeO_2–Fe_2O_3–NiO nanocomposite	0.6 g/L	5 mg/L	sunlight	73% at 50 min	[78]
Fe_2O_3 nanoparticles	0.4 g/L	10 mg/L	sunlight	53% at 50 min	[79]
40CaO–30 B_2O_3-30 V_2O_5	0.5 g/L	10 mg/L	UV light	99% at 180 min	Present work

4. Conclusions

This paper reported a facile synthesis of borovanadate glasses, and the study of the chemical durability and photocatalytic activity of CaO-B_2O_3-V_2O_5 glasses. The substitution by increased B_2O_3 has led to the increase of Tg temperature, leading to a decrease in the dissolution rate, therefore enhancing the chemical durability of the glass. The photocatalytic performance of the prepared glasses was examined under UV irradiation by the degradation of methylene blue (MB) dye. The prepared 40CaO-30B_2O_3-30V_2O_5 photocatalyst with a catalyst loading of 0.5 g/L had the highest photodegradation efficiency of MB (10 mg/L), whereby it reached about 99% after 180 min of irradiation. This study shed light on the importance of glass materials as a sustainable method for the depollution of water through introducing more transition metals (i.e., V_2O_5).

Supplementary Materials: The following supporting information can be downloaded at: https://www.mdpi.com/article/10.3390/catal13030512/s1. Figure S1: Infrared spectra for all the glass samples. Figure S2: Raman spectrum for all the glass samples. Figure S3: Diborovanadates groupements $[B_2V_2O_9]^{2-}$ (according to Reddy et al. [43]). References [80,81] are cited in the Supplementary Materials.

Author Contributions: Writing—original draft, preparation and characterization of materials, and editing, A.K., A.B.A. and G.K.; writing, editing, supervision, validation, and visualization, H.A.A. and A.Z.; supervision, editing, validation, and visualization, A.B.A. and M.S. All authors have read and agreed to the published version of the manuscript.

Funding: This research received no external funding.

Data Availability Statement: Data is available upon a reasonable request.

Acknowledgments: The authors acknowledge the support of Mohammed V University in Rabat, Faculty of Sciences.

Conflicts of Interest: The authors declare no conflict of interest.

References

1. Barebita, H.; Ferraa, S.; Moutataouia, M.; Baach, B.; Elbadaoui, A.; Nimour, A.; Guedira, T. Structural investigation of Bi_2O_3-P_2O_5-B_2O_3-V_2O_5 quaternary glass system by Raman, FTIR and thermal analysis. *Chem. Phys. Lett.* **2020**, *760*, 138031. [CrossRef]
2. Margha, F.H.; Marzouk, M.A. Influence of vanadium addition on the optical and photoluminescence properties of borate glasses and their glass–ceramic derivatives. *Appl. Phys. A* **2019**, *125*, 623. [CrossRef]
3. Hussein, E.M.A. Characterization of Some Chemical and Physical Properties of Lithium Borate Glasses Doped with CuO and/or TeO_2. *J. Chem. Soc. Pak.* **2019**, *41*, 52. [CrossRef]
4. Abdelghany, A.; Hammad, A.H. Impact of vanadium ions in barium borate glass. *Spectrochim. Acta Part A Mol. Biomol. Spectrosc.* **2015**, *137*, 39–44. [CrossRef] [PubMed]
5. Rao, R.B.; Veeraiah, N. Study on some physical properties of Li_2O–MO–B_2O_3: V2O_5 glasses. *Phys. B Condens. Matter* **2004**, *348*, 256–271. [CrossRef]
6. Singh, K.; Ratnam, J. Electrical conductivity of the Li_2O_B_2O_3 system with V_2O_5. *Solid State Ionics* **1988**, *31*, 221–226. [CrossRef]

7. Issever, U.; Kilic, G.; Ilik, E. The Impact of CuO on physical, structural, optical and thermal properties of dark VPB semiconducting glasses. *Opt. Mater.* **2021**, *116*, 111084. [CrossRef]
8. Aly, K.; Hassaan, M.; Saddeek, Y. Thermal features and physical properties of sulfur modified barium vanadate glasses. *Phase Transit.* **2013**, *86*, 477–489. [CrossRef]
9. Singh, G.P.; Kaur, P.; Kaur, S.; Singh, D.P. Role of V_2O_5 in Structural Properties of V_2O_5-MnO_2-PbO-B_2O_3 Glasses. *Mater. Phys. Mech.* **2011**, *12*, 58–63.
10. Reddy, N.S. Role of zinc sulfate on thermal and mechanical properties of borovanadate glasses. *Mater. Today Proc.* **2022**, *49*, 771–776. [CrossRef]
11. Reddy, M.S.; Gowda, V.C.V.; Reddy, C.N.; Tripathi, S.K.; Dharamvir, K.; Kumar, R.; Saini, G.S.S. *Elastic Properties and Structural Studies on Boro-Vanadate Glasses Containing Sulphate (SO_4^{2-}) AIP Conference Proceedings*; American Institute of Physics: College Park, MD, USA, 2011; pp. 209–210. [CrossRef]
12. Kaaouass, A.; Ali, A.B.; Alloun, F.; Zarrouk, A.; Saadi Structural, M. Thermal and Physical Properties of the Calcium Borovanadate Glasses Belonging to the 40CaO-(60-x)B_2O_3-xV_2O_5 System. *Biointerface Res. Appl. Chem.* **2022**, *13*, 48. [CrossRef]
13. Choi, S.; Kim, J.; Jung, J.; Park, H.; Ryu, B. Effect of Substituting B_2O_3 for P_2O_5 in Conductive Vanadate Glass. *J. Korean Ceram. Soc.* **2015**, *52*, 140–145. [CrossRef]
14. Sajid, M.M.; Shad, N.A.; Javed, Y.; Khan, S.B.; Zhang, Z.; Amin, N.; Zhai, H. Preparation and characterization of Vanadium pentoxide (V_2O_5) for photocatalytic degradation of monoazo and diazo dyes. *Surf. Interfaces* **2020**, *19*, 100502. [CrossRef]
15. Ma, G.-Q.; Liu, F.-S.; Wang, S.; Dang, Z.-C.; Zhang, J.-W.; Fu, X.-J.; Hou, M.-S. Preparation and characterization of Bi2S3/3DOM-TiO_2 for efficient photocatalytic degradation of rhodamine B. *Mater. Sci. Semicond. Process.* **2019**, *100*, 61–72. [CrossRef]
16. Chang, Y.; Yu, K.; Zhang, C.; Yang, Z.; Feng, Y.; Hao, H.; Jiang, Y.; Lou, L.-L.; Zhou, W.; Liu, S. Ternary CdS/Au/3DOM-$SrTiO_3$ composites with synergistic enhancement for hydrogen production from visible-light photocatalytic water splitting. *Appl. Catal. B Environ.* **2017**, *215*, 74–84. [CrossRef]
17. Li, G.; Liu, Y. Photocatalytic degradation of methyl orange and gas-sensing performance of nanosized ZnO. *Mater. Sci. Semicond. Process.* **2013**, *16*, 792–796. [CrossRef]
18. Kalnaowakul, P.; Phairatana, T.; Ubolchollakhet, K.; Sangchay, W.; Rodchanarowan, A. Synthesis of Bi_2O_3-doped and TiO_2-doped porous Lava for photocatalytic studies. *Mater. Today: Proc.* **2018**, *5*, 9312–9318. [CrossRef]
19. Kubacka, A.; Fernández-García, M.; Colón, G. Advanced Nanoarchitectures for Solar Photocatalytic Applications. *Chem. Rev.* **2011**, *112*, 1555–1614. [CrossRef]
20. Lopes, E.D.O.; Dallabona, I.D.; Weinschutz, R.; Jorge, R.M.M. Fe/polymer-based photocatalyst synthesized by sono-sorption method applied to wastewater treatment. *J. Photochem. Photobiol. A Chem.* **2020**, *396*, 112545. [CrossRef]
21. Wijetunga, S.; Li, X.-F.; Jian, C. Effect of organic load on decolourization of textile wastewater containing acid dyes in upflow anaerobic sludge blanket reactor. *J. Hazard. Mater.* **2010**, *177*, 792–798. [CrossRef]
22. Ouasfi, N.; Bouzekri, S.; Zbair, M.; Ahsaine, H.A.; Bakkas, S.; Bensitel, M.; Khamliche, L. Carbonaceous material prepared by ultrasonic assisted pyrolysis from algae (*Bifurcaria bifurcata*): Response surface modeling of aspirin removal. *Surf. Interfaces* **2019**, *14*, 61–71. [CrossRef]
23. Nachit, W.; Ahsaine, H.A.; Ramzi, Z.; Touhtouh, S.; Goncharova, I.; Benkhouja, K. Photocatalytic activity of anatase-brookite TiO_2 nanoparticles synthesized by sol gel method at low temperature. *Opt. Mater.* **2022**, *129*, 112256. [CrossRef]
24. Adán, C.; Marugán, J.; Obregón, S.; Colón, G. Photocatalytic activity of bismuth vanadates under UV-A and visible light irradiation: Inactivation of Escherichia coli vs oxidation of methanol. *Catal. Today* **2015**, *240*, 93–99. [CrossRef]
25. Belver, C.; Adán, C.; García-Rodríguez, S.; Fernández-García, M. Photocatalytic behavior of silver vanadates: Microemulsion synthesis and post-reaction characterization. *Chem. Eng. J.* **2013**, *224*, 24–31. [CrossRef]
26. Belver, C.; Adán, C.; Fernández-García, M. Photocatalytic behaviour of Bi_2MO_6 polymetalates for rhodamine B degradation. *Catal. Today* **2009**, *143*, 274–281. [CrossRef]
27. Avansi, W.; de Mendonça, V.R.; Lopes, O.F.; Ribeiro, C. Vanadium pentoxide 1-D nanostructures applied to dye removal from aqueous systems by coupling adsorption and visible-light photodegradation. *RSC Adv.* **2015**, *5*, 12000–12006. [CrossRef]
28. Lotfi, S.; El Ouardi, M.; Ahsaine, H.A.; Assani, A. Recent progress on the synthesis, morphology and photocatalytic dye degradation of $BiVO_4$ photocatalysts: A review, Catalysis Reviews. *Catal. Rev.* **2022**. [CrossRef]
29. Iqbal, M.; Fatima, M.; Javed, T.; Anam, A.; Nazir, A.; Kanwal, Q.; Shehzadi, Z.; I Khan, M.; Nisar, J.; Abbas, M.; et al. Microwave assisted synthesis of zinc vanadate nanoparticles and photocatalytic application. *Mater. Res. Express* **2020**, *7*, 015070. [CrossRef]
30. Ferraa, S.; Naciri, Y.; Hsini, A.; Barebita, H.; Bouziani, A.; Albourine, A.; Nimour, A.; Guedira, T. Evolution of the physicochemical and photocatalytic properties of BaO embedded in bismuth phosphovanadates glasses. *Chem. Phys. Lett.* **2021**, *763*, 138173. [CrossRef]
31. Thakur, V.; Kushwaha, H.; Singh, A.; Vaish, R.; Punia, R.; Singh, L. A study on the structural and photocatalytic degradation of ciprofloxacine using (70B_2O_3–29Bi_2O_3–1Dy_2O_3)–x(BaO–TiO_2) glass ceramics. *J. Non-Cryst. Solids* **2015**, *428*, 197–203. [CrossRef]
32. Sharma, S.K.; Singh, V.P.; Chauhan, V.S.; Kushwaha, H.S.; Vaish, R. Photocatalytic Active Bismuth Fluoride/Oxyfluoride Surface Crystallized 2Bi_2O_3-B_2O_3 Glass–Ceramics. *J. Electron. Mater.* **2018**, *47*, 3490–3496. [CrossRef]
33. Ali, A.S.; Khan, I.; Zhang, B.; Razum, M.; Pavić, L.; Šantić, A.; Bingham, P.A.; Nomura, K.; Kubuki, S. Structural, electrical and photocatalytic properties of iron-containing soda-lime aluminosilicate glass and glass-ceramics. *J. Non-Cryst. Solids* **2021**, *553*, 120510. [CrossRef]

34. Janbandhu, S.; Munishwar, S.; Gedam, R. Synthesis, characterization and photocatalytic degradation efficiency of CdS quantum dots embedded in sodium borosilicate glasses. *Appl. Surf. Sci.* **2018**, *449*, 221–227. [CrossRef]
35. Tupberg, C.; Chandet, N.; Wattanavichan, K.; Randorn, C. Catalytic and antibacterial activities of novel colored zinc borophosphate glasses. *RSC Adv.* **2016**, *6*, 79602–79611. [CrossRef]
36. Sharma, S.K.; Singh, V.P.; Bhargava, A.; Park, S.-H.; Chauhan, V.S.; Vaish, R. Surface crystallization of BiOCl on $2Bi_2O_3$–B_2O_3 glasses for photocatalytic applications. *J. Mater. Sci. Mater. Electron.* **2021**, *32*, 10520–10531. [CrossRef]
37. Khan, I.; Saeed, K.; Zekker, I.; Zhang, B.; Hendi, A.H.; Ahmad, A.; Ahmad, S.; Zada, N.; Ahmad, H.; Shah, L.A.; et al. Review on Methylene Blue: Its Properties, Uses, Toxicity and Photodegradation. *Water* **2022**, *14*, 242. [CrossRef]
38. Houas, A.; Lachheb, H.; Ksibi, M.; Elaloui, E.; Guillard, C.; Herrmann, J.M. Photocatalytic degradation pathway of methylene blue in water. *Appl. Catal. B Environ.* **2001**, *31*, 145–157. [CrossRef]
39. Yuharia, S.F.; Awanga, A.; Rajak, M.A.A.; Dayouc, J. Alteration on the chemical durability of tellurite glass: Effect of heat treatment. *Chalcogenide Lett.* **2021**, *18*, 171–181. [CrossRef]
40. Mahraz, Z.A.S.; Sahar, M.R.; Ghoshal, S.K. IMPROVED CHEMICAL DURABILITY AND THERMAL STABILITY OF ZINC BORO-TELLURITE GLASS. *Chalcogenide Lett.* **2014**, *11*, 453–460.
41. Li, X.; Xiao, Z.; Luo, M.; Dong, X.; Du, T.; Wang, Y. Low melting glasses in ZnO-Fe_2O_3-P_2O_5 system with high chemical durability and thermal stability for sealing or waste immobilization. *J. Non-Cryst. Solids* **2017**, *469*, 62–69. [CrossRef]
42. Saudi, H.A.; El-Kameesy, S.U. Investigation of modified zinc borate glasses doped with BaO as a nuclear radiation-shielding material. *Radiat. Detect. Technol. Methods* **2018**, *2*, 44. [CrossRef]
43. Reddy, C.N.; Gowda, V.V.; Chakradhar, R.S. Elastic properties and structural studies on lead–boro–vanadate glasses. *J. Non-Cryst. Solids* **2008**, *354*, 32–40. [CrossRef]
44. Viswanatha, R.; Reddy, M.V.S.; Reddy, C.N.; Chakradhar, R.S. Infrared and MAS NMR studies of potassium borovanadate glasses. *J. Mol. Struct.* **2008**, *889*, 197–203. [CrossRef]
45. Li, H.; Lin, H.; Chen, W.; Luo, L. IR and Raman investigation on the structure of (100-x)[$0.33B_2O_3$–$0.67ZnO$]–xV_2O_5 glasses. *J. Non-Cryst. Solids* **2006**, *352*, 3069–3073. [CrossRef]
46. Kenanakis, G.; Katsarakis, N. Chemically grown TiO_2 on glass with superior photocatalytic properties. *J. Environ. Chem. Eng.* **2014**, *2*, 1748–1755. [CrossRef]
47. de Oliveira Guidolin, T.; Possolli, N.M.; Polla, M.B.; Wermuth, T.B.; de Oliveira, T.F.; Eller, S.; Montedo, O.R.K.; Arcaro, S.; Cechinel, M.A.P. Photocatalytic pathway on the degradation of methylene blue from aqueous solutions using magnetite nanoparticles. *J. Clean. Prod.* **2021**, *318*, 128556. [CrossRef]
48. Mahanta, U.; Khandelwal, M.; Deshpande, A.S. TiO_2@SiO_2 nanoparticles for methylene blue removal and photocatalytic degradation under natural sunlight and low-power UV light. *Appl. Surf. Sci.* **2022**, *576*, 151745. [CrossRef]
49. Que, V.N.X.; Khoi, T.T.; Thuy, N.T.; Dung, T.T.M.; Binh, D.T.T.; Huy, N.N. Factors Determining the Removal Efficiency of Procion MX in Waters Using Titanate Nanotubes Catalyzed by UV Irradiation. *J. Nanotechnol.* **2021**, *2021*, 8870453. [CrossRef]
50. Ahmina, W.; El Moudane, M.; Shaim, A.; Zriouil, M.; Taibi, M. Chemical durability, electrical and dielectric properties of the ternary system (50-x)K_2O–xMnO–$50P_2O_5$ phosphate glasses. *Mater. Today: Proc.* **2019**, *13*, 466–473. [CrossRef]
51. Laourayed, M.; El Moudane, M.; Khachani, M.; Boudalia, M.; Guenbour, A.; Bellaouchou, A.; Tabyaoui, M. Effect of the Bi_2O_3 on the thermal, structural and chemical durability of some bismuth niobium phosphate glasses. *Mater. Today: Proc.* **2019**, *13*, 974–981. [CrossRef]
52. Ahmina, W.; El Moudane, M.; Zriouil, M.; Cherraj, M.; Taibi, M. Study of the mechanical and chemical properties of potassium manganese phosphate glasses. *MATEC Web Conf.* **2018**, *149*, 01081. [CrossRef]
53. Kim, N.-J.; Im, S.-H.; Kim, N.-H.; Yoon, D.-K.; Ryu, B.-K. Structure and Properties of Borophosphate Glasses. *Electron. Mater. Lett.* **2010**, *6*, 103–106. [CrossRef]
54. Han, K.; Hwang, C.; Kim, D.; Gwoo, D.; Kim, T.; Choi, W.; Kee, K.; Kim, J.; Ryu, B. Effects of substituting B_2O_3 for P_2O_5 on the structures and properties of V_2O_5-P_2O_5 glass systems. *Electron. Mater. Lett.* **2012**, *8*, 655–658. [CrossRef]
55. Ba, K.; Chahine, A.; Touhami, M.E.; Jermoumi, T.; Shaim, A. Elaboration and characterization of new glasses with high chemical durability in the system (70-x)TiO_2-xNiO-$30P_2O_5$. *Mater. Res. Innov.* **2022**, *26*, 100–106. [CrossRef]
56. Li, X.; Yang, H.; Song, X.; Wu, Y. Glass forming region, structure and properties of zinc iron phosphate glasses. *J. Non-Cryst. Solids* **2013**, *379*, 208–213. [CrossRef]
57. Es-Soufi, H.; Bih, L. Effect of TiO_2 on the chemical durability and optical properties of Mo-based phosphate glasses. *J. Non-Cryst. Solids* **2021**, *558*, 120655. [CrossRef]
58. Yuvasree, P.; Nithya, K.; Neelakandeswari, N.; Rajasekaran, N.; Uthayarani, K.; Chitra, M.; Kumar, S.S. Phytochemical Preparation, Characterization and Photocatalytic Applications of Ag-TiO_2 Nanocatalyst. *Adv. Mater. Res.* **2015**, *1086*, 1–6. [CrossRef]
59. Shaim, A.; Amaterz, E.; Naciri, Y.; Taoufyq, A.; Bakiz, B.; Ezahri, M.; Benlhachemi, A.; Ouammou, A.; Chahine, A. Synthesis, characterization and photocatalytic activity of titano-phosphate glasses. *Mediterr. J. Chem.* **2019**, *8*, 66–73. [CrossRef]
60. Fu, J. Photocatalytic properties of glass ceramics containing anatase-type TiO_2. *Mater. Lett.* **2012**, *68*, 419–422. [CrossRef]
61. Dong, H.; Zuo, Y.; Song, N.; Hong, S.; Xiao, M.; Zhu, D.; Sun, J.; Chen, G.; Li, C. Bimetallic synergetic regulating effect on electronic structure in cobalt/vanadium co-doped carbon nitride for boosting photocatalytic performance. *Appl. Catal. B Environ.* **2021**, *287*, 119954. [CrossRef]

62. Lin, W.-C.; Lin, Y.-J. Effect of Vanadium(IV)-Doping on the Visible Light-Induced Catalytic Activity of Titanium Dioxide Catalysts for Methylene Blue Degradation. *Environ. Eng. Sci.* **2012**, *29*, 447–452. [CrossRef]
63. Nešić, J.; Manojlović, D.D.; Anđelković, I.; Dojčinović, B.P.; Vulić, P.J.; Krstić, J.; Roglić, G.M. Preparation, characterization and photocatalytic activity of lanthanum and vanadium co-doped mesoporous TiO_2 for azo-dye degradation. *J. Mol. Catal. A Chem.* **2013**, *378*, 67–75. [CrossRef]
64. Unal, F.A.; Ok, S.; Unal, M.; Topal, S.; Cellat, K.; Şen, F. Synthesis, characterization, and application of transition metals (Ni, Zr, and Fe) doped TiO_2 photoelectrodes for dye-sensitized solar cells. *J. Mol. Liq.* **2020**, *299*, 112177. [CrossRef]
65. Naciri, Y.; Hsini, A.; Ajmal, Z.; Bouddouch, A.; Bakiz, B.; Navío, J.; Albourine, A.; Valmalette, J.-C.; Ezahri, M.; Benlhachemi, A. Influence of Sr-doping on structural, optical and photocatalytic properties of synthesized $Ca_3(PO_4)_2$. *J. Colloid Interface Sci.* **2020**, *572*, 269–280. [CrossRef] [PubMed]
66. Naciri, Y.; Bouddouch, A.; Bakiz, B.; Taoufyq, A.; Ezahri, M.; Benlhachemi, A. Photocatalytic degradation of sulfadiazine by $Zn_3(PO_4)_2/BiPO_4$ composites upon UV light irradiation. *Mater. Today: Proc.* **2019**, *22*, 48–51. [CrossRef]
67. Barebita, H.; Naciri, Y.; Ferraa, S.; Nimour, A.; Guedira, T. Investigation of structural and photocatalytic behavior of Bi13B1-2xVxPxO20.95+2x ($0 \leq x \leq 0.5$). *Solid State Sci.* **2020**, *108*, 106389. [CrossRef]
68. Zhang, D.; Liu, F.-S.; Wang, S.; Li, Z.; Qian, Q.-Q.; Wang, X.-Q.; Si, G.-L. Preparation and properties of CuO/Zn Cd1−S photocatalysts. *Mater. Sci. Semicond. Process.* **2015**, *40*, 602–612. [CrossRef]
69. Ahsaine, H.A. UV-light photocatalytic properties of the bismuth lutetium tungstate system Bi2-xLuxWO6 ($0 \leq x \leq 1$). *Mater. Lett.* **2020**, *276*, 128221. [CrossRef]
70. Ahsaine, H.A.; Slassi, A.; Naciri, Y.; Chennah, A.; Jaramillo-Páez, C.; Anfar, Z.; Zbair, M.; Benlhachemi, A.; Navío, J.A. Photo/Electrocatalytic Properties of Nanocrystalline ZnO and La–Doped ZnO: Combined DFT Fundamental Semiconducting Properties and Experimental Study. *Chemistryselect* **2018**, *3*, 7778–7791. [CrossRef]
71. Naciri, Y.; Ahsaine, H.A.; Chennah, A.; Amedlous, A.; Taoufyq, A.; Bakiz, B.; Ezahri, M.; Villain, S.; Benlhachemi, A. Facile synthesis, characterization and photocatalytic performance of $Zn_3(PO_4)_2$ platelets toward photodegradation of Rhodamine B dye. *J. Environ. Chem. Eng.* **2018**, *6*, 1840–1847. [CrossRef]
72. Ahsaine, H.A.; El Jaouhari, A.; Slassi, A.; Ezahri, M.; Benlhachemi, A.; Bakiz, B.; Guinneton, F.; Gavarri, J.-R. Electronic band structure and visible-light photocatalytic activity of Bi_2WO_6: Elucidating the effect of lutetium doping. *RSC Adv.* **2016**, *6*, 101105–101114. [CrossRef]
73. Sajid, M.M.; Khan, S.B.; Shad, N.A.; Amin, N. Synthesis of $Zn_3(VO_4)_2/BiVO_4$ heterojunction composite for the photocatalytic degradation of methylene blue organic dye and electrochemical detection of H_2O_2. *RSC Adv.* **2018**, *8*, 35403–35412. [CrossRef] [PubMed]
74. Abdullah, A.H. Degradation of Methylene Blue Dye by CuO-$BiVO_4$ Photocatalysts under Visible Light Irradiation. *Malays. J. Anal. Sci.* **2016**, *20*, 1338–1345. [CrossRef]
75. Pu, Y.; Wang, J.; Huang, Y.; Chen, C.; Kim, S.I.; Seo, H.J. Visible-Light-Induced Degradation of Methylene Blue by $SrBi_3VO_8$ Nanoparticles. *J. Am. Ceram. Soc.* **2015**, *98*, 2528–2533. [CrossRef]
76. Salhi, A.; Aarfane, A.; Tahiri, S.; Khamliche, L.; Bensitel, M.; Bentiss, F.; El Krati, M. Study of the photocatalytic degradation of methylene blue dye using titanium-doped hydroxyapatite. *Mediterr. J. Chem.* **2015**, *4*, 59–67. [CrossRef]
77. Nisa, M.U.; Abid, A.G.; Gouadria, S.; Munawar, T.; Alrowaili, Z.; Abdullah, M.; Al-Buriahi, M.; Iqbal, F.; Ehsan, M.F.; Ashiq, M.N. Boosted electron-transfer/separation of $SnO_2/CdSe/Bi_2S_3$ heterostructure for excellent photocatalytic degradation of organic dye pollutants under visible light. *Surf. Interfaces* **2022**, *31*, 102012. [CrossRef]
78. Mukhtar, F.; Munawar, T.; Nadeem, M.S.; Rehman, M.N.U.; Khan, S.A.; Koc, M.; Batool, S.; Hasan, M.; Iqbal, F. Dual Z-scheme core-shell PANI-CeO_2-Fe_2O_3-NiO heterostructured nanocomposite for dyes remediation under sunlight and bacterial disinfection. *Environ. Res.* **2022**, *215*, 114140. [CrossRef]
79. Mukhtar, F.; Munawar, T.; Nadeem, M.S.; Khan, S.A.; Koc, M.; Batool, S.; Hasan, M.; Iqbal, F. Enhanced sunlight-absorption of Fe_2O_3 covered by PANI for the photodegradation of organic pollutants and antimicrobial inactivation. *Adv. Powder Technol.* **2022**, *33*, 103708. [CrossRef]
80. Narayana Reddy, C.; Damle, R.; Anavekar, R.V. Spectroscopic and structural studies on calcium borate glasses containing V_2O_5. *Phys. Chem. Glasses-Eur. J. Glass Sci. Technol. Part B* **2006**, *47*, 34–40.
81. Hübert, T.; Mosel, G.; Witke, K. Structural Elements in Borovanadate Glasses. *Glass Phys. Chem.* **2001**, *27*, 114–120. [CrossRef]